Available online at www.sciencedirect.com
SCIENCE DIRECT®
Journal of Sound and Vibration 288 (2005) 829–845
JOURNAL OF SOUND AND VIBRATION
www.elsevier.com/locate/jsvi

Finite element analysis of resonant sloshing response in 2-D baffled tank

J.R. Cho*, H.W. Lee, S.Y. Ha

School of Mechanical Engineering, Pusan National University, Kumjung-Ku, Busan 609-735, Korea

Received 22 July 2003; received in revised form 8 October 2004; accepted 13 January 2005
Available online 28 April 2005

Abstract

This paper is concerned with the numerical analysis of the resonance characteristics of liquid sloshing in a 2-D baffled tank subjected to the forced lateral excitation. Sloshing flow is formulated based on the linearized potential flow theory, while an artificial damping term is employed into the kinematic free-surface condition to reflect the eminent dissipation effect in resonant sloshing. A test FEM program is developed for the resonant sloshing analysis in frequency domain. The choice of the artificial damping coefficient is parametrically examined and the numerical accuracy is verified through the comparison with the available analytic solutions. Through the numerical analysis of sloshing frequency response with respect to the number, location and opening width of baffle, the sloshing damping characteristics by the baffle are parametrically investigated.

1. Introduction

The liquid in containers displays a free-surface fluctuation when the container is subjected to an external excitation like earthquake and this liquid sloshing may be a direct or indirect cause of the unexpected instability and failure of structural systems equipped with the liquid container. As either the excitation amplitude increases or the excitation frequency approaches the natural sloshing frequency, the damage caused by liquid sloshing may become fatal. This hazardous

*Corresponding author. Tel.: +82 51 514 7640.
E-mail address: jrcho@hyowon.pusan.ac.kr (J.R. Cho).

0022-460X/$ - see front matter © 2005 Elsevier Ltd. All rights reserved.
doi:10.1016/j.jsv.2005.01.019

situation is involved in a wide field of engineering applications, such as above-ground liquid-storage tanks under earthquake waves [1–3], fuel storage tanks of aerospace vehicles [4,5] and cargo tanks of LNG carriers in service [6]. Thus, the sloshing suppression has become an inevitable research subject in the community associated with the fluid sloshing during several decades [7–11].

Usually, the sloshing effect is suppressed in a passive manner [10] by introducing additional sub-structures called baffle or sloshing damper [12] into the containers. The shape and design concept of the sloshing damper varies depending on the sloshing motion type, the kind of external excitation and the container shape [13–15]. Representative examples of the sloshing damper are annular ring baffle installed slightly below the liquid free surface, semi-spherical obstacles installed at the bottom plate of container, wedge with holes installed inclined to the flow direction. The basic concept of passive sloshing damper is to dissipate the sloshing motion energy by breaking a main sloshing flow into several weaker sub-streams. The reader may refer to our previous works [11,15] for illustration of the fuel sloshing suppression in moving tanks by flexible annular ring baffle.

In the resonant sloshing analysis, the damping effect should not be ignored in order to prevent the divergence in the frequency response near resonance frequencies. However, differing from the numerical sloshing analysis in time domain [15,16], a consideration of full viscous flow for the case in frequency domain leads to complicated and large-scale matrix equations in the form of complex variable. In order to reflect the damping effect while assuming inviscid liquid flow, Faltinsen [17] proposed an artificial dissipation mechanism based on the Rayleigh damping concept. A product of the artificial viscosity coefficient and the velocity potential gradient is added into the Euler equation, from which the kinematic free-surface condition with the artificial damping term is derived through a modified Bernoulli equation, Where, the artificial viscosity coefficient is defined by the relative damping ratio to the critical damping. On the other hand, in the analytical analysis for the sloshing frequency response in baffled containers, a modified velocity potential function is usually employed with the help of the power series expansion method, in order to take the viscosity effect into consideration [13].

As an extension of our previous works [11,14,15] on the liquid sloshing in baffled tanks, this paper is intended to investigate the resonance frequency response of liquid sloshing in baffled 2-D tank by a finite element method. While employing the kinematic free-surface condition with the artificial damping term, we formulate the resonance frequency response according to the linearized potential flow theory. The reliability of the numerical solutions is assessed by the comparison with the analytical solutions [17], and the artificial damping coefficient is parametrically examined. The effects of baffle on the resonance sloshing response are investigated with respect to the major baffle parameters.

2. Sloshing problem with artificial damping

Fig. 1 shows a two-dimensional rectangular tank with a pair of baffles in which interior liquid is filled up to the height H_L from the tank bottom in the stationary condition. Both tank and baffle are assumed to be rigid, and the horizontal harmonic excitation is applied to the whole tank. The reader may refer to Ref. [11] for the flexible baffled tank and Ref. [18] for the structure flexibility

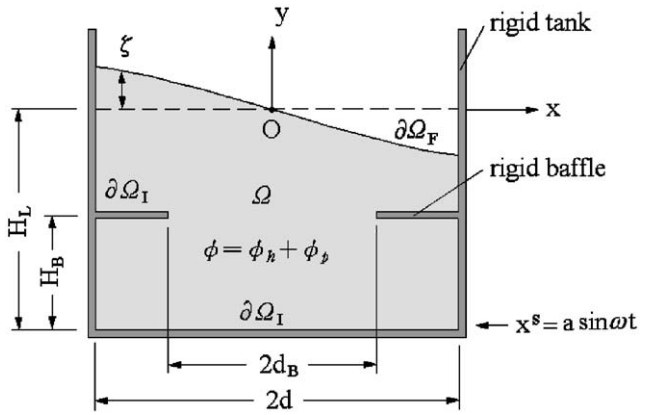

Fig. 1. Liquid sloshing in 2-D baffled tank by horizontal harmonic excitation.

effect on the liquid sloshing. A Cartesian coordinate system is originated at the center of the undisturbed free surface. Even though the baffle thickness is neglected, the boundary of the liquid domain Ω is composed of the liquid–structure interface $\partial\Omega_I$ and the free surface $\partial\Omega_F$, as depicted in Fig. 1.

We assume the liquid is inviscid incompressible and the sloshing flow irrotational so that there exists a velocity potential function ϕ satisfying

$$\nabla^2\phi = 0 \quad \text{in } \Omega, \tag{1}$$

with a boundary condition on the structure–liquid interface

$$\nabla\phi \cdot \mathbf{n} = \mathbf{u}^s \cdot \mathbf{n} \quad \text{on } \partial\Omega_I. \tag{2}$$

Here, $\mathbf{n}$ denotes the outward unit vector normal to the liquid boundary and $\mathbf{u}^s = \{a\omega \cos \omega t, 0\}$ is the tank velocity. To the free surface, we specify the linearized dynamic and kinematic conditions given by

$$\frac{\partial\phi}{\partial t} + g\zeta + \mu\phi = 0 \quad \text{on } \partial\Omega_F, \tag{3}$$

$$\frac{\partial\phi}{\partial y} = \frac{\partial\zeta}{\partial t} \quad \text{on } \partial\Omega_F, \tag{4}$$

where ζ is the elevation of liquid free surface. Meanwhile, the term $\mu\phi$ is nothing but the artificial damping introduced to prevent the divergence phenomenon at resonance frequencies. In fact, the potential theory cannot predict the energy dissipation in sloshing flow, so the numerical divergence occurs owing to the non-vanishing transient response with the time lapse. By taking time derivative to Eq. (3) together with the relation (4) leads to a unified free-surface condition given by

$$\frac{\partial^2\phi}{\partial t^2} + g\frac{\partial\phi}{\partial y} + \mu\frac{\partial\phi}{\partial t} = 0 \quad \text{on } \partial\Omega_F. \tag{5}$$

Meanwhile, the hydrodynamic pressure p and the free-surface elevation ζ in the linearized sloshing flow with the artificial surface damping are calculated according to

$$p = -\rho\left(\frac{\partial\phi}{\partial t} + \mu\phi\right) \quad \text{in } \Omega, \tag{6}$$

$$\zeta = -\frac{1}{g}\left(\frac{\partial\phi}{\partial t} + \mu\phi\right) \quad \text{on } \partial\Omega_F. \tag{7}$$

And, the horizontal dynamic force resultant F_x acting on the tank, the most dominant dynamic force resultant in the current case, is computed through

$$F_x = \int_{-H_L}^{0} [p(d, y) - p(-d, y)]\,\mathrm{d}y. \tag{8}$$

For reference, the velocity potential can be decomposed into two parts, ϕ_h of the relative liquid flow to the tank and ϕ_p of the tank motion such that

$$\phi = \phi_h + \phi_p, \qquad \phi_p = a\omega x \cos\omega t. \tag{9}$$

Substituting Eq. (9) into Eqs. (1), (2) and (5), one can easily derive the linearized potential flow problem with the artificial surface damping:

$$\nabla^2\phi_h = 0 \quad \text{in } \Omega, \tag{10}$$

with the boundary and free-surface conditions

$$\nabla\phi_h \cdot \mathbf{n} = 0 \quad \text{on } \partial\Omega_I, \tag{11}$$

$$\frac{\partial^2\phi_h}{\partial t^2} + g\,\frac{\partial\phi_h}{\partial y} + \mu\frac{\partial\phi_h}{\partial t} = x(a\omega^3 x\cos\omega t + \mu a\omega^2 \sin\omega t) \quad \text{on } \partial\Omega_F. \tag{12}$$

The separation of the total velocity potential in this manner is convenient for the analytical sloshing resonance analysis summarized in Appendix A.

3. Finite element approximation in frequency domain

Differing from the analytical derivation, we approximate the total velocity potential ϕ for the numerical analysis of the free-surface elevation, the hydrodynamic pressure and the dynamic force resultant interested in the current study. By applying the virtual work principle to Eq. (1), together with the boundary conditions in Eqs. (2) and (5), we can obtain the variational formulation: Find $\dot{\phi}$ such that

$$\begin{aligned}\int_\Omega \nabla\phi\cdot\nabla\psi\,\mathrm{d}\Omega = &-\frac{1}{g}\int_{\partial\Omega_F}\frac{\partial^2\phi}{\partial t^2}\psi\,\mathrm{d}s - \frac{\mu}{g}\int_{\partial\Omega_F}\frac{\partial\phi}{\partial t}\psi\,\mathrm{d}s \\ &+ a\omega\cos\omega t\int_{\partial\Omega_I^R}\psi\,\mathrm{d}s - a\omega\cos\omega t\int_{\partial\Omega_I^L}\psi\,\mathrm{d}s\end{aligned} \tag{13}$$

for every admissible velocity potential ψ. Here, $\partial\Omega_I^R$ denotes the right-side wall and $\partial\Omega_I^L$ the left-side wall of the tank.

Because the external excitation $\mathbf{u}^S$ is a cosine function, while restricting to the steady-state response, we can let ϕ be in function of cosine with the phase angle β. Using 9-node iso-parametric basis functions $\{N_i\}_{i=1}^N$ we expand trial and test functions

$$\phi = \sum_{i=1}^{N} N_i \bar{\phi}_i \cos(\omega t - \beta), \tag{14}$$

$$\psi = \sum_{i=1}^{N} N_i \bar{\psi}_i \cos(\omega t - \beta). \tag{15}$$

Then, the previous variational formulation ends up with the matrix equations given by

$$[\mathbf{K} - \omega^2 \mathbf{M}]\bar{\phi} \cos(\omega t - \beta) - \omega \mathbf{C}\bar{\phi} \sin(\omega t - \beta) = \omega \mathbf{F} \cos \omega t, \tag{16}$$

where $\bar{\phi}$ is defined by the vector of nodal velocity potentials. The matrices in Eq. (16) are defined by

$$\mathbf{K} = \int_{\Omega} (\nabla \mathbf{N})^{\mathrm{T}} (\nabla \mathbf{N}) \, \mathrm{d}\Omega, \tag{17}$$

$$\mathbf{M} = \frac{1}{g} \int_{\partial\Omega_F} \mathbf{N}^{\mathrm{T}} \mathbf{N} \, \mathrm{d}s, \tag{18}$$

$$\mathbf{F} = a \int_{\partial\Omega_I^R} \mathbf{N}^{\mathrm{T}} \, \mathrm{d}s - a \int_{\partial\Omega_I^L} \mathbf{N}^{\mathrm{T}} \, \mathrm{d}s, \tag{19}$$

with $\mathbf{C} = \mu\mathbf{M}$.

In order to establish the modal equations of Eq. (16), we first compute the natural sloshing frequencies and modes with

$$[\mathbf{K} - \omega^2 \mathbf{M}]\bar{\phi} = 0. \tag{20}$$

Realizing that the mass matrix $\mathbf{M}$ is restricted only to the finite element nodes of the liquid free surface $\partial\Omega_F$, Eq. (20) can be decomposed as follows [2,3,18]:

$$\begin{bmatrix} \mathbf{K}_{SS} & \mathbf{K}_{SI} \\ \mathbf{K}_{IS} & \mathbf{K}_{II} \end{bmatrix} \begin{Bmatrix} \bar{\phi}_S \\ \bar{\phi}_I \end{Bmatrix} - \omega^2 \begin{bmatrix} \mathbf{M} & 0 \\ 0 & 0 \end{bmatrix} \begin{Bmatrix} \bar{\phi}_S \\ \bar{\phi}_I \end{Bmatrix} = \begin{Bmatrix} 0 \\ 0 \end{Bmatrix}. \tag{21}$$

where subscripts S and I are used to stand for the sub-matrices and the sub-vectors associated, respectively, with the free-surface nodes and the remaining interior liquid nodes. For instance, $\mathbf{K}_{\mathrm{SI}}$ is the sub-matrix made with the free-surface nodes (for the test potential ψ) and the remaining interior nodes (for the trial potential ϕ).

It is worth noting that the number $N_S < N$ of natural frequencies becomes identical with the free-surface node number such that only the natural frequencies corresponding to the free-surface sloshing come out. This is because we neglect the flexibility of tank and baffles. Referring to our previous paper [18], the mass matrix in Eq. (21) becomes full when the structure flexibility is

considered, so that both the sloshing mode and the side bulging mode do appear. Here, the side bulging modes refer to the natural modes of flexible tank.

According to the static condensation we obtain the reduced eigen matrix equations for the free-surface sloshing given by

$$[\mathbf{K}_{SS} - \mathbf{K}_{SI}\mathbf{K}_{II}^{-1}\mathbf{K}_{IS}]\bar{\phi}_S - \omega^2\mathbf{M}\bar{\phi}_S = 0. \tag{22}$$

After computing a set of natural frequencies $\{\omega_n^i\}$ and partial natural modes $\{\bar{\phi}_S^i\}$, we obtain the remaining parts $\bar{\phi}_I$ of the full natural modes using

$$\bar{\phi}_I = -\mathbf{K}_{II}^{-1}\mathbf{K}_{IS}\bar{\phi}_S. \tag{23}$$

Next, we expand the nodal potential vector $\bar{\phi}$ in terms of only the sine modes among N_S natural modes such that

$$\bar{\phi}(\mathbf{x};\omega) = \sum_{i=1}^{N_S^*} \bar{\phi}_n^i(\mathbf{x}) \cdot q_i(\omega), \tag{24}$$

where q_i are defined as the modal participation coefficients to be determined. Substituting Eq. (24) into (16) and premultiplying the resulting equation by $(\bar{\phi}_n^k)^{\mathrm{T}}$ leads to N_S^* uncoupled modal equations for $\{q_k\}$:

$$[(\omega_n^k)^2 - \omega^2]q_k \cos(\omega t - \beta) - \omega\mu q_k \sin(\omega t - \beta) = \omega Q_k \cos \omega t, \tag{25}$$

with $Q_k = (\bar{\phi}_n^k)^{\mathrm{T}}\mathbf{F}$. Here, the M-orthonormality of natural modes (i.e. $(\bar{\phi}_n^i)^{\mathrm{T}}\mathbf{M}\bar{\phi}_n^j = \delta_{ij}$) and the definition of the matrix $\mathbf{C}$ are used.

According to the basic relation of triangular functions to Eq. (25), we can derive two equations given by

$$[((\omega_n^k)^2 - \omega^2)\cos\beta + \omega\mu \sin\beta]q_k = \omega Q_k, \tag{26}$$

$$[((\omega_n^k)^2 - \omega^2)\sin\beta - \omega\mu \cos\beta]q_k = 0. \tag{27}$$

As a result, the angles and participation coefficients are determined according to

$$\beta_k = \tan^{-1}\left(\frac{\mu\omega}{(\omega_n^k)^2 - \omega^2}\right), \qquad -\frac{\pi}{2} < \beta < \frac{\pi}{2}, \tag{28}$$

$$q_k = \frac{\pm\omega Q_k}{\left[((\omega_n^k)^2 - \omega^2)^2 + (\mu\omega)^2\right]^{1/2}}, \tag{29}$$

where q_k is positive when $\omega_n > \omega$ and vice versa. Then, we finally have the finite element approximation of the total velocity potential given by

$$\phi = \sum_{i=1}^{N} N_i \left(\sum_{k=1}^{N_S^*} q_k \bar{\phi}_n^k \cos(\omega t - \beta_k)\right)_i. \tag{30}$$

It is worth noting that the phase angle is frequency dependent.

4. Numerical experiments

We developed a PC-based test FEM program coded in Fortran according to the theoretical results described so far, in which mass matrix is not lumped so that its upper triangular part is stored. Meanwhile, the full reduced eigenmatrix system (22) is solved by Jacobi iteration method without truncating using the Lanczos transformation because the matrix size is not large. As mentioned before, its size is identical with the number of free-surface nodes.

Through preliminary experiments, while being limited to the case without baffle, we verify the reliability of the test program by comparing it with the analytical solutions and examine the parametric effect of the artificial damping coefficient. Than, we perform the numerical experiments of baffled tank with respect to the number, the installation height and the opening width of baffle, in order to examine the parametric effects of baffle.

4.1. Preliminary results

We first consider a liquid-storage tank without baffle under the horizontal harmonic excitation $x^S = a \sin \omega t$. Geometry, material and excitation data for preliminary experiments are recorded in Table 1, where the excitation frequency ω taken as an input variable is varying with the increment $\Delta\omega$ of 0.001 rad/s. Meanwhile, the relative damping ratio is taken as a variable for the parametric investigation. The liquid domain Ω is uniformly discretized with 9-node quadratic elements such that the total element number is 300 (20 in the horizontal direction $\times$ 15 in the vertical direction). Then, the number N_S of free-surface nodes becomes 41 so that the reduced eigenmatrix (22) is of size 41×41. We confirmed that this mesh partition shows the relative numerical error less than 1% up to the tenth lowest natural frequencies when compared to the analytical solutions. Analytical derivation of natural sloshing frequencies is well addressed in our previous paper [11].

Fig. 2 presents the frequency response of the relative free-surface elevation ζ/a to the artificial damping ratio μ. For this, only the sine modes among N_S natural sloshing modes are used for the modal expansion in Eq. (24) and the free-surface elevation is taken at the left end of free surface (i.e. at $x = -d$). As shown in Fig. 2(a), the free-surface elevation without damping shows the critical resonance response diverging to infinity at natural sloshing frequencies ($\omega_n^1 = 3.917\,\text{rad/s}$, $\omega_n^2 = 6.798\,\text{rad/s}$ and $\omega_n^3 = 8.776\,\text{rad/s}$). However, from Figs. 2(b)–(d), we can see that the damping effect in the sloshing response in proportion to the artificial damping ratio, so that the introduction of the artificial damping term into the free-surface condition effectively reflects the dissipation effect in the resonant sloshing. Meanwhile, one can confirm the

Table 1
Simulation data taken for the verification experiments

Liquid in tank		External excitation	
Liquid width ($2d$) (m)	2.0	Excitation amplitude (a) (m)	1.0 (E−02)
Liquid height (H_L) (m)	1.0	Excitation frequency (ω) (rad/s)	Variable
Liquid density (ρ) (kg/m^3)	1.0 (E+03)	Relative damping ratio (μ)	Variable

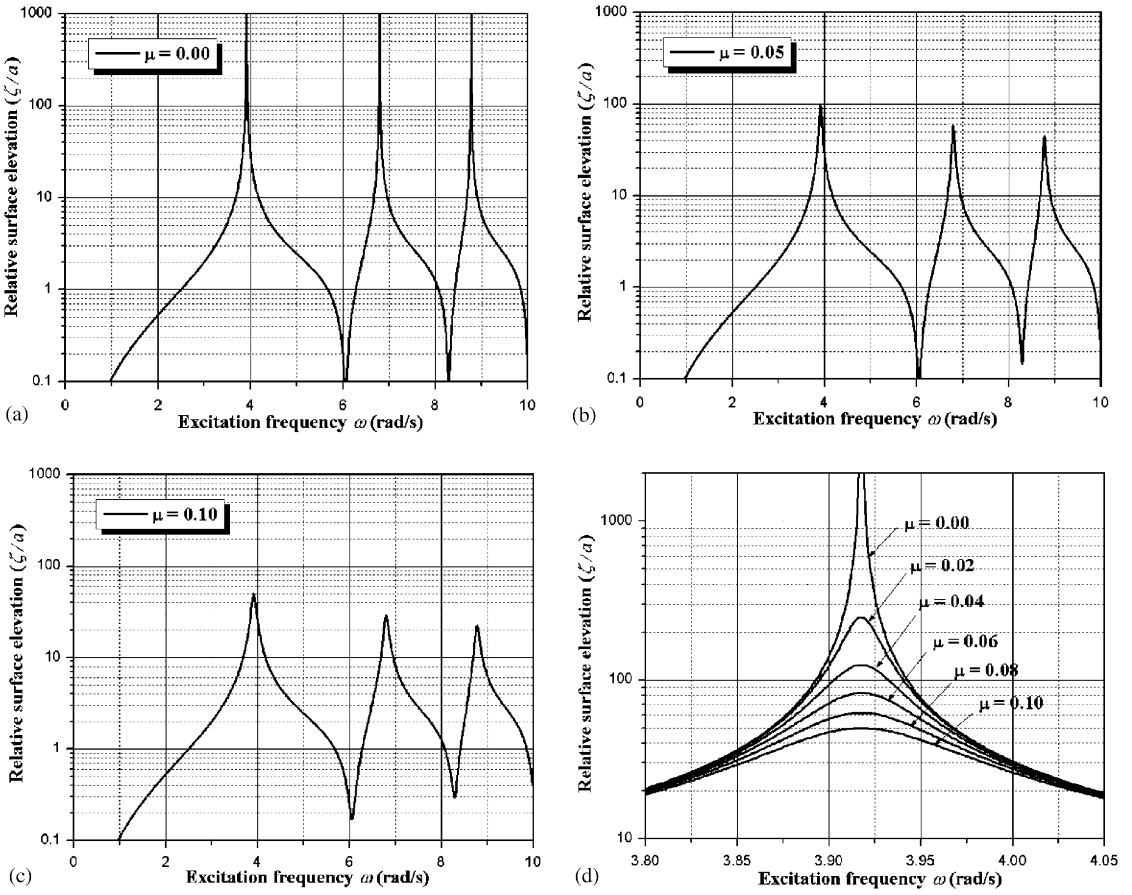

Fig. 2. Frequency response of the free-surface elevation ζ to the relative damping ratio: (a) $\mu = 0$, (b) $\mu = 0.05$, (c) $\mu = 0.1$; and (d) near the fundamental resonance frequency.

highest resonance response at the fundamental sloshing frequency for a specific damping ratio. Also, the hydrodynamic pressure and the dynamic resultant force did exhibit similar frequency responses to the damping ratio.

Fig. 3 shows the comparison of frequency responses with the analytical solutions obtained according to the formulae given in Appendix A, up to the seventh resonance frequencies. We include 100 terms in the series expansions for the analytic solutions, and we take the hydrodynamic pressure at the same point as for the free-surface elevation (i.e. at $x = -d$). Meanwhile, we set the artificial damping ratio μ to 0.05 and calibrate three observation quantities for easy comparison throughout this paper. By examining the plots in Fig. 3, one can confirm that both analytic and numerical results are in excellent agreement up to the resonance frequency of observation. Referring to the comparison given in Table 2, the relative error in the peak sloshing frequency response estimated with respect to the analytic solution is less than 2% up to the second resonance frequency. However, the relative error becomes larger with the resonance frequency

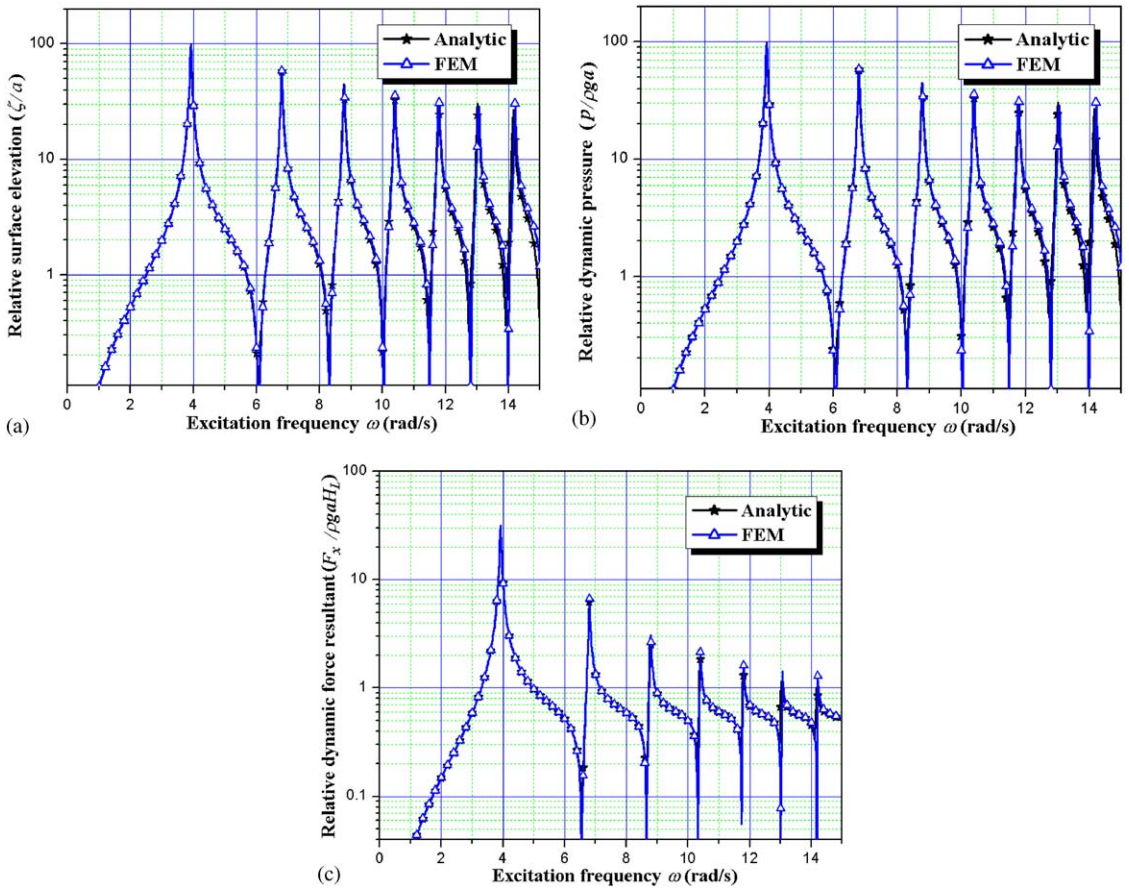

Fig. 3. Comparison with analytical solutions ($\mu = 0.05$): (a) free-surface elevation ζ/a; (b) hydrodynamic pressure $p/\rho ga$; and (c) horizontal dynamic force resultant $F_x/\rho gaH_L$.

Table 2
Comparison of peak responses between analytical and FEM at first and second resonance frequencies ($\mu = 0.05$)

Resonance frequency		$(\zeta/a)_{\text{peak}}$	$(p/\rho ga)_{\text{peak}}$	$(F_x/2\rho gaH_L)$
First	Analytic	99.388	99.429	31.533
	FEM	99.714	99.714	31.551
	Error (%)	0.33	0.29	0.06
Second	Analytic	57.753	57.862	6.202
	FEM	58.830	58.830	6.714
	Error (%)	1.83	1.64	1.62

increase, because the numerical error involved in the natural frequencies and modes obtained by FEM inherently increases as the natural frequency becomes higher.

Fig. 4(a) shows the frequency response of free-surface elevation near the fundamental resonance frequency to the relative liquid fill height $H_L/2d$. The peak surface elevation and the

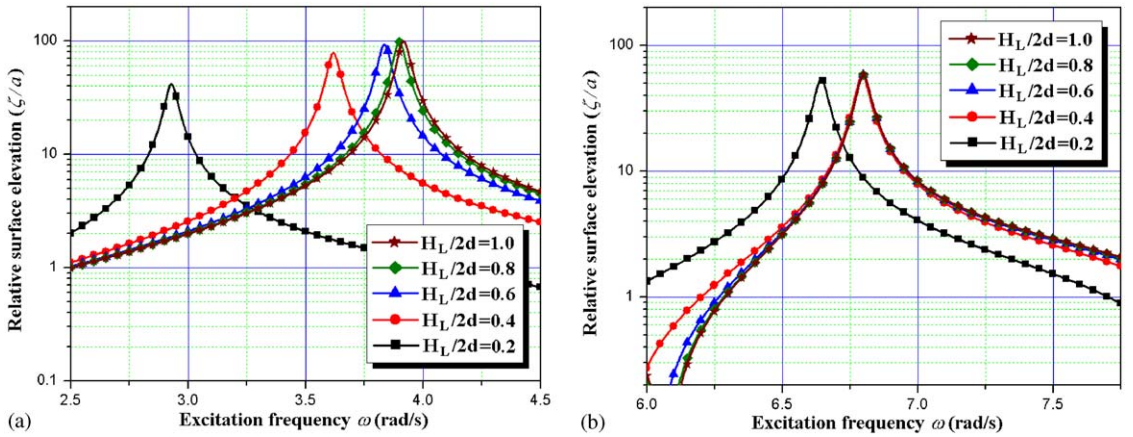

Fig. 4. Relative free-surface elevation to the liquid fill height ($\mu = 0.05$): (a) near fundamental resonance frequency; and (b) near second resonance frequency.

fundamental resonance frequency increase in proportional to the liquid fill height, but the dependence on the liquid fill height becomes dull as $H_L/2d$ approaches unity. This result is consistent with the fact that only the upper liquid region participates in the liquid sloshing motion [1,2,11,18]. On the other hand, as given in Fig. 4(b), the difference in resonant sloshing by the liquid fill height becomes smaller at the second resonance frequency. This implies that the liquid fill height gives rise to the dominant effect in the resonance response at the fundamental frequency.

4.2. Parametric results

We next consider the baffled cases in which the number, the installation height and the opening width of baffle are taken variable while keeping the other simulation data in Table 1 unchanged. Also, the mesh partition and the artificial damping ratio are same as in the preliminary experiment (i.e. 20×15 and $\mu = 0.05$). Referring to Fig. 5, baffles are installed with uniform vertical spacing with respect to the liquid fill height, and the occurrence of zero-thickness baffle is numerically implemented by separating liquid nodes [11].

The effect of the baffle number on the frequency response of free-surface elevation near the fundamental resonance frequency is presented in Fig. 6(a). The relative opening width d_B/d of baffle is set by 0.5. Together with the baffle number, the resonance frequency and the peak elevation height show a uniform decrease. Thus, we can obtain the sloshing suppression improvement by increasing the baffle number, which agrees with our previous work on baffled fuel tanks subject to the vertical acceleration [15]. v, this trend suggests that one can control the fundamental resonance frequency by adjusting the baffle number.

Due to the flow separation by baffle (even though partially), above and below the baffle, the effective value of the relative liquid fill height $H_L/2d$ becomes smaller with the baffle number increase. In view of the parametric results in Fig. 4 regarding the relative liquid fill height, the

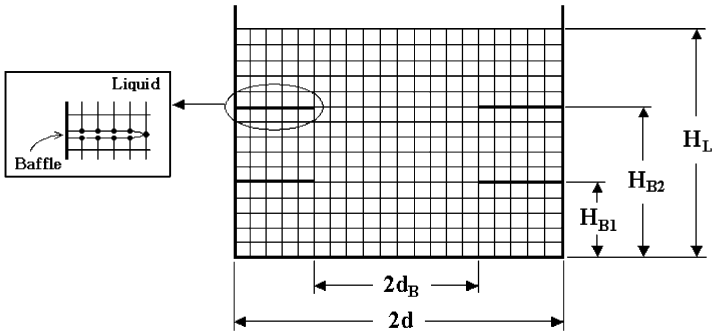

Fig. 5. Finite element mesh for the baffled case.

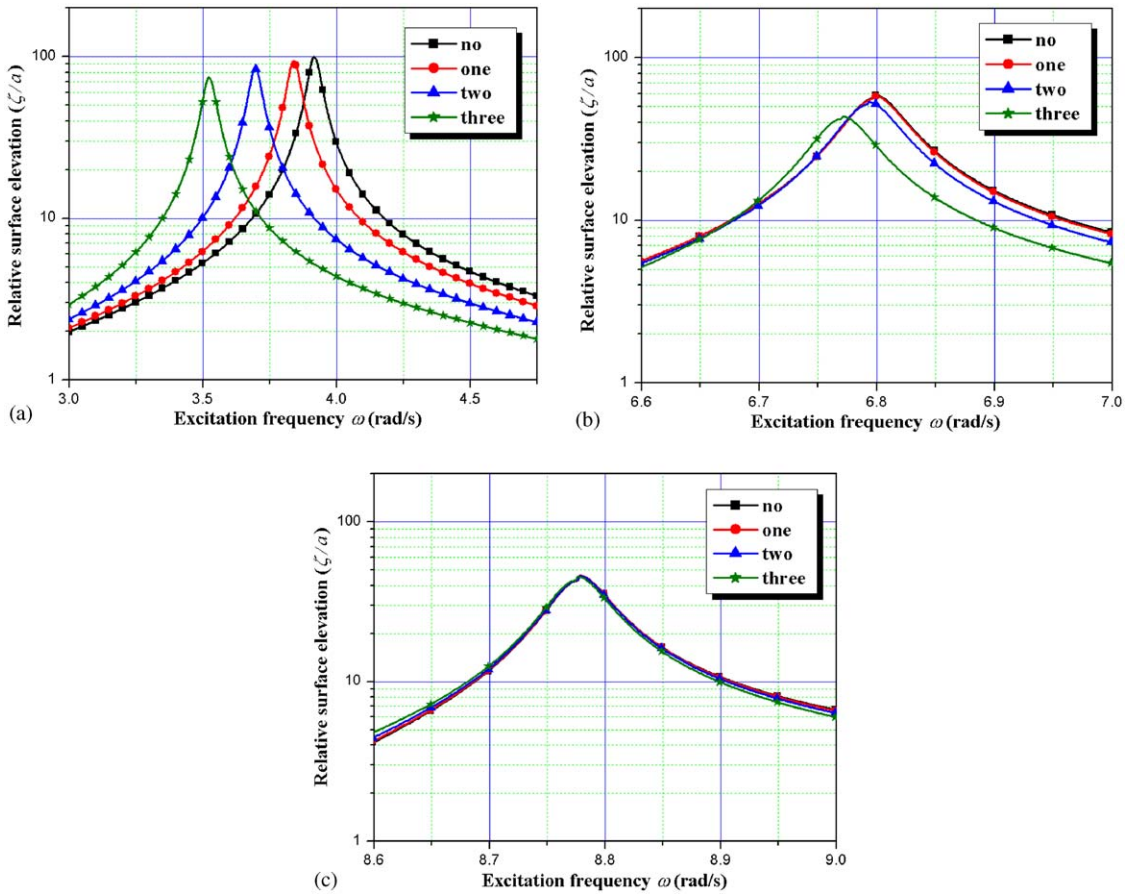

Fig. 6. Frequency response of the free-surface elevation to the baffle number ($d_B/d = 0.5$): (a) near fundamental resonance frequency; (b) near second resonance frequency; and (c) near third resonance frequency.

reduction of fundamental resonance frequency to the baffle number is natural. On the other hand, referring to Figs. 6(b) and (c), the difference in the baffle number becomes negligible as the resonance frequency becomes higher.

We next consider one-baffle case with $\mu = 0.05$ in order to examine the parametric effects of the baffle height and the baffle opening width on the resonance sloshing response. Fig. 7(a) depicts the parametric variation of the free-surface elevation near the fundamental resonance frequency with respect to the relative baffle height when $d_B/d = 0.5$. The peak elevation height and the resonance frequency reduce in proportion to the baffle installation height, and the reduction ratio becomes higher as baffle approaches the liquid free surface. The importance of the baffle height is apparent at the second resonance frequency, as shown in Fig. 7(b), such that the resonance response displays a big difference above and below $H_B/H_L = 0.7$. This trend does appear up to the third resonance frequency, so that the importance of the baffle installation height is clear. In addition, one can effectively improve the sloshing damping performance by installing the baffle near the free surface, which is also consistent well with the numerical results by Gedikli and Erguven [10] and Cho and Lee [15].

Referring to Fig. 8(a), the reduction of baffle opening width leads to the uniform decrease of the fundamental resonance frequency and the peak elevation height. It is because the liquid flow separation above and below the baffle strengthens with the baffle opening reduction so that the liquid amount participating in the sloshing motion becomes smaller. And, which in turn gives rise

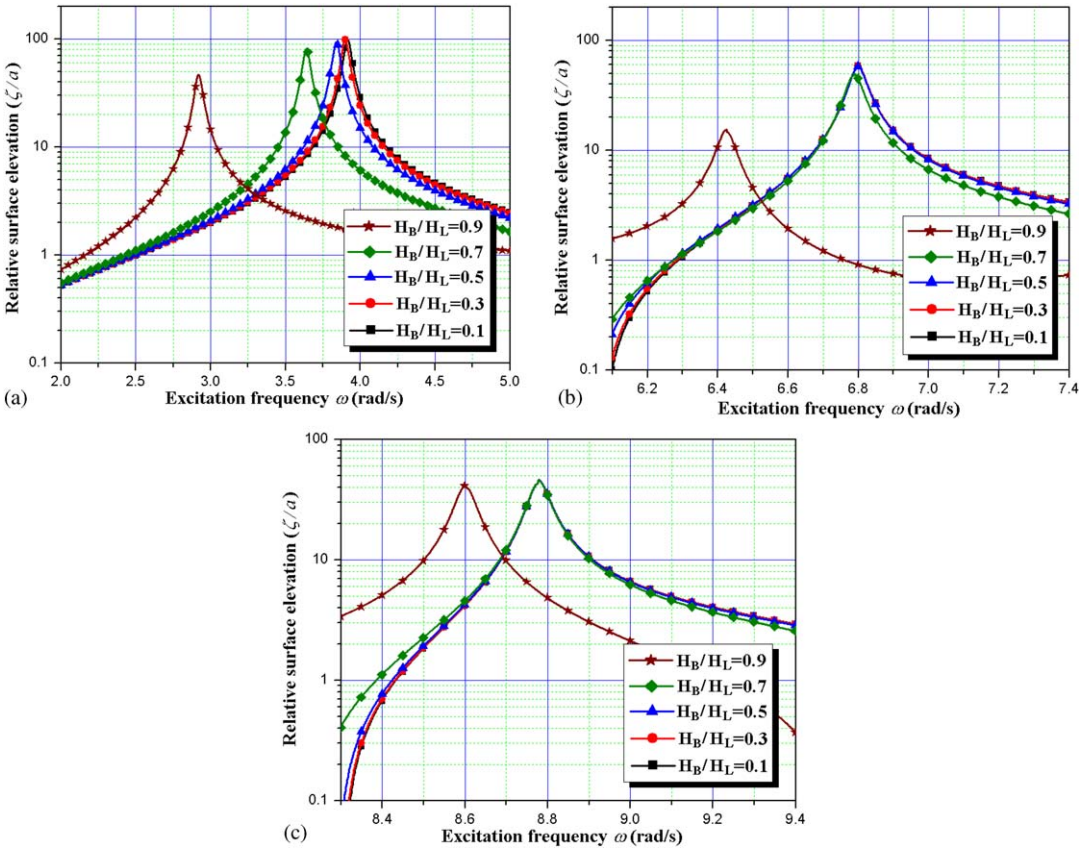

Fig. 7. Frequency response of the free-surface elevation to the baffle height (one baffle with $d_B/d = 0.5$): (a) near fundamental resonance frequency; (b) near second resonance frequency; and (c) near third resonance frequency.

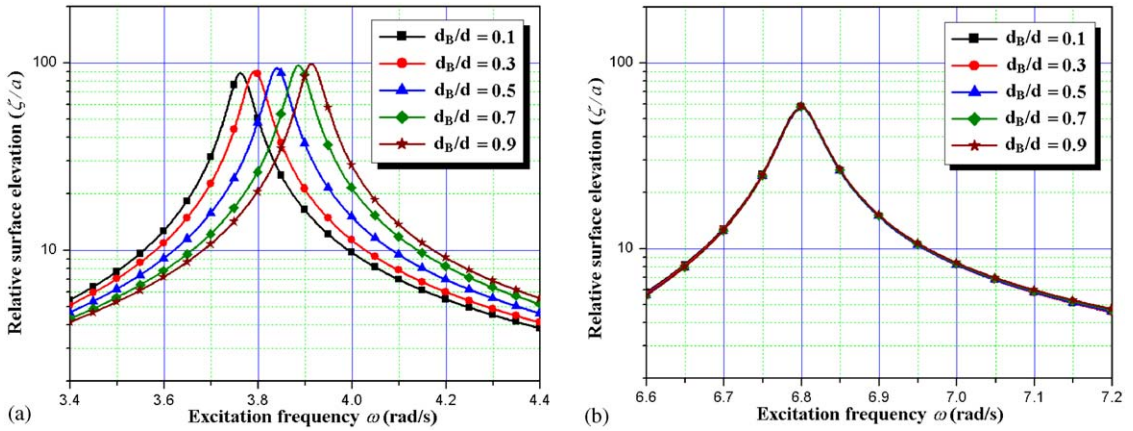

Fig. 8. Frequency response of the free-surface elevation to the opening width (one baffle installed at $H_B/H_L = 0.5$): (a) near fundamental resonance frequency; and (b) near second resonance frequency.

to the effect decreasing the relative liquid fill height $H_L/2d$. However, the effect of the baffle opening width is relatively weak, compared to the other two baffle parameters. Furthermore, as presented in Fig. 8(b), any notable difference between baffle opening widths is not shown any more at the second resonance frequency.

The variation of fundamental resonance frequency to the opening width and the installation height is summarized in Figs. 9(a) and (b), respectively. The fundamental resonance frequency shows the monotonic decrease with the reduction of d_B/d or the increase of H_B/H_L from which one can find out that the baffle should be installed just below the free surface and its opening width is recommendable to be as small as possible for the damping performance maximization.

5. Concluding remarks

The resonance sloshing response of liquid contained in 2-D baffled tank subject to the lateral harmonic excitation has been numerically investigated. We confirmed the validity of the artificial damping introduced into the kinematic surface condition to reflect the eminent dissipation effect in the resonant liquid sloshing. While being restricted to the no-baffle case, the numerical accuracy has been verified according to the comparison with the analytic solutions derived by the separation of variables. Meanwhile, the parametric effects of the liquid fill height, the baffle number, the opening width and the baffle location have been parametrically examined.

According to the parametric experiments on the resonance sloshing response the following main observations are drawn:

1. The fundamental resonance frequency and the peak elevation height uniformly decreases with the baffle number, the baffle installation height, and the reduction of the baffle opening width and the liquid fill height. Also, these parameters give rise to the same trend in the hydrodynamic pressure and the dynamic force resultant.

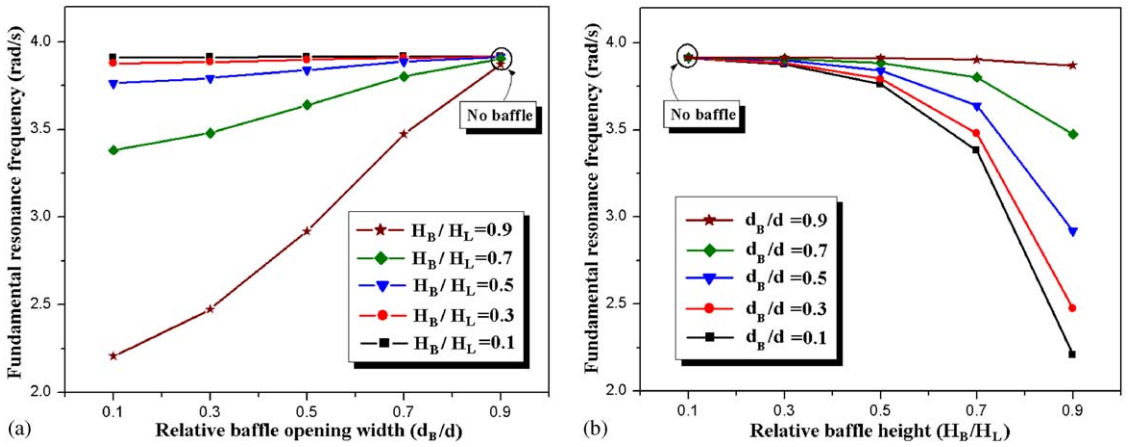

Fig. 9. Variation of fundamental resonance frequency (one-baffle case): (a) to the baffle opening width; and (b) to the baffle height.

2. The effect of these four parameters on the resonance sloshing response becomes as a whole weaker as the resonance frequency goes higher. Thus, the fundamental sloshing resonance causing the dominant damage on liquid–structure systems can be successfully suppressed by the passive baffle.
3. Meanwhile, among four parameters, we observed that the influence of the baffle installation height is largest.

As a result, one can adjust the fundamental resonance frequency of liquid sloshing with the passive baffle to make it suitable to the structural system containing the liquid-storage tank, together with the remarkable reduction of the resonance amplitude.

Acknowledgement

This work was supported by Korea Science & Engineering Foundation under Grant No. R05-2004-000-117.

Appendix. Analytic solution for no baffle case

For the case without baffle, the velocity potential ϕ_h governed by Eqs. (10)–(12) can be analytically derived by the separation of variables. Plugging $\phi_h(x,y;t) = X(x)Y(y)T(t)$ into Eq. (10) produces

$$\frac{d^2X}{dx^2} + k^2X = 0, \qquad \frac{d^2Y}{dy^2} - k^2Y = 0, \tag{A.1}$$

with the separation constant k. Applying the boundary condition (11) specified on $\partial\Omega_I$ to the solution of Eq. (A.1) gives us

$$\phi_h = \sum_{n=0}^{\infty} \sin\, k_n x \cosh k_n(y + H_L) T_n(t), \tag{A.2}$$

where $k_n = (2n+1)\pi/2d$.

Substituting Eq. (A.2) into the free-surface boundary condition (12), together with the Fourier series expansion of x, leads to

$$\frac{\mathrm{d}^2 T_n}{\mathrm{d}t^2} + \mu \frac{\mathrm{d}T_n}{\mathrm{d}t} + \omega_n^2 T_n = (\omega \cos \omega t + \mu \sin \omega t) F_n, \tag{A.3}$$

with

$$\omega_n = g k_n \tanh k_n H_L, \tag{A.4}$$

$$F_n = \frac{2}{d} \frac{(-1)^n}{k_n^2} \frac{a\omega^2}{\cosh k_n H_L}. \tag{A.5}$$

Along the straightforward procedure one can easily obtain the general solution of Eq. (A.3) given by

$$T_n = \mathrm{e}^{-(\mu/2)t}(E_{1n} \cos B_n t + E_{2n} \sin B_n t) + C_n \cos \omega t + D_n \sin \omega t, \tag{A.6}$$

where

$$B_n = \sqrt{\omega_n^2 - \frac{\mu}{4}}, \tag{A.7}$$

$$C_n = \frac{(\omega_n^2 - \omega^2)^2 \omega F_n - \mu^2 \omega F_n}{(\omega_n^2 - \omega^2)^2 + (\mu\omega)^2}, \tag{A.8}$$

$$D_n = \frac{(\omega_n^2 - \omega^2)^2 \mu F_n - \mu \omega^2 F_n}{(\omega_n^2 - \omega^2)^2 + (\mu\omega)^2}. \tag{A.9}$$

Plugging Eq. (A.6) into Eq. (A.2) and combining with ϕ_p in Eq. (8) finally leads to

$$\begin{aligned} \phi &= \phi_h + \phi_p \\ &= \sum_{n=0}^{\infty} \sin\, k_n x \cosh\, k_n(y + H_L)[\mathrm{e}^{-(\mu/2)t}(E_{1n} \cos\, B_n t + E_{2n} \sin\, B_n t) \\ &\quad + C_n \cos\, \omega t + D_n \sin\, \omega t] + \frac{a}{\omega} \sum_{n=0}^{\infty} \sin\, k_n x \cosh\, k_n H_L \cos\, \omega t. \end{aligned} \tag{A.10}$$

Here, the coefficients E_{1n} and E_{2n} are determined using the initial conditions: $\phi = \partial\phi/\partial t = 0$ on the liquid free surface $\partial\Omega_F$ such that

$$E_{1n} = -C_n - \frac{F_n}{\omega^2}, \tag{A.11}$$

$$E_{2n} = -\frac{\mu E_{1n}/2 - \omega D_n}{\sqrt{\omega_n^2 - \mu^2/4}}. \tag{A.12}$$

Substituting Eq. (A.10) into Eqs. (6) and (7) and taking only the steady-state responses, we have

$$\zeta_{st} = -\frac{1}{g}\sqrt{Z_1^2 + Z_2^2}\cos(\omega t - \varphi), \tag{A.13}$$

$$p_{st} = \rho g \zeta_{st}, \tag{A.14}$$

where φ is the phase angle and

$$Z_1 = \sum_{n=0}^{\infty} \sin\, k_n x \cosh\, k_n H_L \left(\mu C_n + \omega D_n + \frac{\mu F_n}{\omega}\right), \tag{A.15}$$

$$Z_2 = \sum_{n=0}^{\infty} \sin\, k_n x \cosh\, k_n H_L (\mu D_n + \omega C_n - F_n). \tag{A.16}$$

On the other hand, the steady-state response of the horizontal dynamic force resultant F_x is computed according to

$$F_x = \sqrt{F_1^2 + F_2^2}\cos(\omega t - \varphi), \tag{A.17}$$

with

$$F_1 = -2\rho \sum_{n=0}^{\infty} \frac{1}{k_n} \sin\, k_n x (\cosh\, k_n H_L - 1)\left(\mu C_n + \omega D_n + \frac{\mu F_n}{\omega}\right), \tag{A.18}$$

$$F_2 = -2\rho \sum_{n=0}^{\infty} \frac{1}{k_n} \sin\, k_n x (\cosh\, k_n H_L - 1)(\mu D_n + \omega C_n - F_n). \tag{A.19}$$

References

[1] M.A. Haroun, Vibration studies and tests of liquid storage tanks, *Earthquake Engineering and Structural Dynamics* 11 (1983) 179–206.

[2] J.R. Cho, J.M. Song, J.K. Lee, Finite element techniques for the free-vibration and seismic analysis of liquid-storage tanks, *Finite Elements in Analysis and Design* 37 (2001) 467–483.

[3] J.R. Cho, J.K. Lee, J.M. Song, S.H. Park, J.N. Lee, Free vibration analysis of aboveground LNG-storage tanks by the finite element method, *KSME International Journal* 14 (6) (2002) 633–644.

[4] E.W. Graham, A.M. Rodriguez, The characteristics of fuel motion which affects airplane dynamics, *Journal of Applied Mechanics* 19 (1952) 381–388.

[5] H.F. Baur, Nonlinear mechanical model for the description of propellant sloshing, *AIAA Journal* 4 (9) (1966) 1662–1668.

[6] R.L. Bass, E.B. Bowles, P.A. Cox, Liquid dynamic loads in LNG cargo tanks, *SNAME Transactions* 88 (1980) 103–126.

[7] A.M. Siveira, D.G. Stephens, H.W. Leonard, An experimental investigation of liquid oscillation in tanks with various baffles, NASA Technical Note D-715, 1961.

[8] H.N. Abramson, L.R. Garza, Some measurements of the effects of ring baffles in cylindrical tanks, *Journal of Spacecraft Rockets* 1 (5) (1964) 560–764.
[9] D.V. Evans, P. McIver, Resonant frequencies in a container with a vertical baffle, *Journal of Fluid Mechanics* 175 (1987) 295–307.
[10] A. Gedikli, M.E. Erguven, Seismic analysis of a liquid storage tank with a baffle, *Journal of Sound and Vibration* 223 (1) (1999) 141–155.
[11] J.R. Cho, H.W. Lee, K. W. Kim. Free vibration analysis of baffled liquid-storage tanks by the structural-acoustic finite element formulation, *Journal of Sound and Vibration* 258 (5) (2002) 847–866.
[12] V.J. Modi, A. Akinturk, An efficient liquid sloshing damper for control of wind-induced instabilities, *Journal of Wind Engineering and Industrial Aerodynamics* 90 (2002) 1907–1918.
[13] F. Welt, V.J. Modi, Vibration damping through liquid sloshing, Part I: a nonlinear analysis, *Journal of Vibration and Acoustics* 114 (1992) 10–16.
[14] S.Y. Lee, J.R. Cho, Baffled fuel-storage container: parametric study on transient dynamic characteristics, *Structural Engineering and Mechanics* 13 (6) (2002) 653–670.
[15] J.R. Cho, S.Y. Lee, Dynamic analysis of baffled fuel-storage tanks using the ALE finite element method, *International Journal for Numerical Methods in Fluids* 41 (2003) 185–208.
[16] M. Hayashi, K. Hatanaka, M. Kawahara, Lagrangian finite element method for free surface Navier–Stokes flow using fractional step methods, *International Journal for Numerical Methods in Fluids* 13 (1991) 805–840.
[17] O.M. Faltinsen, A numerical nonlinear method of sloshing in tanks with two-dimensional flow, *Journal of Ship Research* 22 (3) (1978) 193–202.
[18] J.R. Cho, J.M. Song, Assessment of classical numerical models for the separate fluid-structure modal analysis, *Journal of Sound and Vibration* 239 (5) (2001) 995–1012.